Onset of Hydrodynamic Mix in High-Velocity, Highly Compressed Inertial Confinement Fusion Implosions

T. Ma,[1] P. K. Patel,[1] N. Izumi,[1] P. T. Springer,[1] M. H. Key,[1] L. J. Atherton,[1] L. R. Benedetti,[1] D. K. Bradley,[1] D. A. Callahan,[1] P. M. Celliers,[1] C. J. Cerjan,[1] D. S. Clark,[1] E. L. Dewald,[1] S. N. Dixit,[1] T. Döppner,[1] D. H. Edgell,[2] R. Epstein,[2] S. Glenn,[1] G. Grim,[3] S. W. Haan,[1] B. A. Hammel,[1] D. Hicks,[1] W. W. Hsing,[1] O. S. Jones,[1] S. F. Khan,[1] J. D. Kilkenny,[4] J. L. Kline,[3] G. A. Kyrala,[3] O. L. Landen,[1] S. Le Pape,[1] B. J. MacGowan,[1] A. J. Mackinnon,[1] A. G. MacPhee,[1] N. B. Meezan,[1] J. D. Moody,[1] A. Pak,[1] T. Parham,[1] H.-S. Park,[1] J. E. Ralph,[1] S. P. Regan,[2] B. A. Remington,[1] H. F. Robey,[1] J. S. Ross,[1] B. K. Spears,[1] V. Smalyuk,[1] L. J. Suter,[1] R. Tommasini,[1] R. P. Town,[1] S. V. Weber,[1] J. D. Lindl,[1] M. J. Edwards,[1] S. H. Glenzer,[1] and E. I. Moses[1]

[1]*Lawrence Livermore National Laboratory, Livermore, California 94550, USA*
[2]*Laboratory for Laser Energetics, University of Rochester, Rochester, New York 14623, USA*
[3]*Los Alamos National Laboratory, Los Alamos, New Mexico 87545, USA*
[4]*General Atomics, San Diego, California 92186, USA*

(Received 25 February 2013; published 23 August 2013)

Deuterium-tritium inertial confinement fusion implosion experiments on the National Ignition Facility have demonstrated yields ranging from 0.8 to 7×10^{14}, and record fuel areal densities of 0.7 to 1.3 g/cm^2. These implosions use hohlraums irradiated with shaped laser pulses of 1.5–1.9 MJ energy. The laser peak power and duration at peak power were varied, as were the capsule ablator dopant concentrations and shell thicknesses. We quantify the level of hydrodynamic instability mix of the ablator into the hot spot from the measured elevated absolute x-ray emission of the hot spot. We observe that DT neutron yield and ion temperature decrease abruptly as the hot spot mix mass increases above several hundred ng. The comparison with radiation-hydrodynamic modeling indicates that low mode asymmetries and increased ablator surface perturbations may be responsible for the current performance.

DOI: 10.1103/PhysRevLett.111.085004 PACS numbers: 52.57.Fg, 52.70.La

Current inertial confinement fusion (ICF) experiments [1,2] conducted on the National Ignition Facility (NIF) [3] seek to indirectly drive a spherical implosion to ignite deuterium-tritium fuel. In this scheme, lasers irradiate the inner wall of a high-Z hohlraum, producing a soft x-ray drive with a Planckian spectrum of 300 eV temperature that ablates and compresses the fuel capsule. Ignition and high fusion yield >1 MJ will occur when the thermonuclear fuel is assembled in a low adiabat, high convergence implosion to high areal density ($\rho R > 1.4$ g/cm^2) enclosing a central hot spot of temperature >4 keV and $\rho R >$ 0.3 g/cm^2. At this stage, alpha deposition further heats the hot spot and generates a self-sustaining burn wave that is launched into the fuel [4–6]. The strategy to achieve these conditions for ignition is outlined in a series of articles by Edwards, Landen, Haan, and co-workers [2,7,8].

The implosions employ a tailored laser pulse with a sequence of four distinct steps, producing four shocks that successively merge until all coalesce just inside the inner radius of the ice. With each shock merger, compression and the shock velocity are both increased [9,10]. The ablation pressure following the fourth shock accelerates the shell inwards, to reach a peak velocity of 370 km/s.

Hydrodynamic instabilities, such as the Rayleigh-Taylor (RT) [11,12], Richtmyer-Meshkov [13,14], and Kelvin-Helmoltz [15,16] instabilities can degrade ICF capsule performance. These instabilities have been studied extensively in direct and indirect drive, and in a variety of geometries; much of the large body of work is reviewed in [17,18]. The evolution of instabilities is sensitive to the ablation rate and surface characteristics [19], with the dominant concern for ICF being ablation-front RT [20]. For ignition experiments, the tradeoff is between implosion velocity, which continues to increase as more mass is ablated, and the penetration of ablator material into the fuel by outer surface imperfections that grow at the ablation front due to the RT instability [21,22]. This growth can also seed perturbations at the fuel-ablator interface, which in turn become RT unstable during deceleration and stagnation. In situations with large RT growth, the ablator may mix into the DT fuel layer and hot spot, increasing the radiative cooling and degrading performance. Previously, germanium x-ray spectroscopy had been used to infer the mix of targets with a Ge dopant layer in the ablator [23]. In the fall of 2011, the Ge was replaced by silicon, which demonstrated improved radiation absorption and higher implosion velocity. Since Si has no high energy x-ray lines that can penetrate the ablator, all of the radiated emission is continuum.

In this Letter, we present a series of experiments conducted at the NIF that show the sensitivity of performance to the level of ablator–hot spot mix. We have developed a simple model that infers the level of DT hot spot contamination from higher Z ablator material by the ratio of the

measured x-ray emission to the calculated emission based on the neutron yield and hot spot temperature. The DT yield and ion temperature decrease nearly monotonically with increasing levels of mix mass. By incorporating artificially enhanced mix, or low mode asymmetries and increased surface perturbations, 2D radiation-hydrodynamic simulations are approaching the experimental results.

Figure 1 illustrates an ignition hohlraum heated by 192 laser beams with typical laser pulse shapes shown where peak power and drive duration are varied. The lasers deliver a total energy of 1.5–1.9 MJ, with peak power ranging from 320–470 TW, at a wavelength of 351 nm. The targets were of the nominal Rev. 5 ignition design [8] using equimolar mixtures of DT cryogenically prepared as a solid 69 μm-thick ice layer with a fuel mass of 170 μg encircling a DT gas mass of 1 μg, all encased in a plastic (CH) shell. This CH ablator had a thickness of 195 μm (T0) or 215 μm (T1), and was doped with trace amounts of silicon, with an outside diameter of 2.26 mm. Implosions were carried out using both gold and depleted uranium (DU) hohlraums, of either 5.44 or 5.75 mm diameter.

At stagnation, the hot spot reaches temperatures of several keV, and emits ~100 J of x rays, the spectral and spatial variation of which contains key information that we use to evaluate the implosion performance. Any ablator material that is mixed into the compressed fuel will equilibrate with the hot spot, and as the ablator is primarily composed of higher Z CH, will radiatively cool the hot spot, reducing the ion temperature and decreasing the neutron yield.

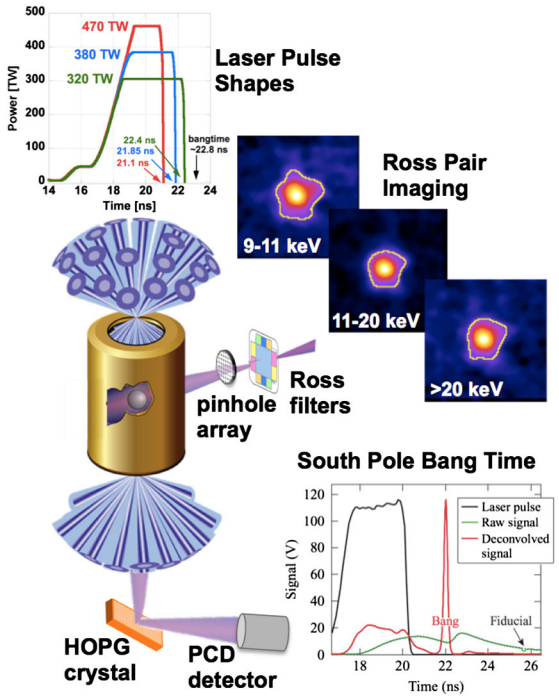

FIG. 1 (color online). Schematic of an ignition target with an example of the laser pulse shapes used. Viewing the implosion through a diagnostic patch in the hohlraum, the Ross filters [32,33] image the temperature- and density-sensitive x-ray emission. The SPBT diagnostic [36,37] views the implosion through the lower hohlraum laser entrance hole.

The model quantifies the ablator mix into the hot spot by determining the individual contributions of DT and CH to the radiated free-free and free-bound emission. The total neutron yield Y_{DT} from the fusion reaction $\mathrm{D} + \mathrm{T} \rightarrow {}^4\mathrm{He}\,(3.5\ \mathrm{MeV}) + n\,(14.1\ \mathrm{MeV})$ is given by

$$Y_{\mathrm{DT}} = n_D n_T \langle \sigma_{\mathrm{DT}} v(T_i) \rangle V \Delta t, \\ = f_D f_T \frac{A_v^2}{\bar{A}^2} \rho_{\mathrm{DT}}^2 \langle \sigma_{\mathrm{DT}} v(T_i) \rangle V \Delta t, \quad (1)$$

where n_D and n_T are the number densities of deuterium and tritium ions, respectively, and f_D and f_T their corresponding atomic fractions; A_v is Avogadro's number; $\bar{A}$ the mean atomic mass; ρ_{DT} the density; $\langle \sigma_{\mathrm{DT}} v(T_i) \rangle$ the DT reactivity cross section at the ion temperature T_i; V the hot spot volume; and Δt the burn duration.

The x-ray emission from the hot spot in the optically thin limit can be written as

$$X_\nu = 4\pi j_{\mathrm{DT}} \times \left(1 + \sum x_i Z_i\right)\left(1 + \sum x_i \frac{j_i}{j_{\mathrm{DT}}}\right) e^{-\tau_\nu^{\mathrm{shell}}} \\ \times V \Delta t (\mathrm{erg/Hz}), \quad (2)$$

where j_{DT} is the total DT emissivity [see Eq. (3)]; j_i is the total emissivity of ion i; the term $(1 + \sum x_i Z_i)[1 + \sum x_i (j_i/j_{\mathrm{DT}})]$ represents the enhancement in emission due to mix of ions with atomic number Z_i, and fraction x_i of the total number of D + T atoms; and $\tau_\nu^{\mathrm{shell}}$ is the optical depth of the shell [5,24]. The free-free continuum emission scales as Z^2, while free-bound emission scales as Z^4.

The DT emission coefficients are obtained from Kirchoff's law and a fit to the OPAL [25] and DCA [26] opacity tables

$$j_{\mathrm{DT}} = \alpha_\nu B_\nu(T_e) \simeq \frac{\rho_{\mathrm{DT}}^2}{\bar{A}^2} \frac{e^{-h\nu/kT_e}}{(h\nu)^{0.33}} (\mathrm{erg/s/cm^3/sr/Hz}), \quad (3)$$

where α_ν is the absorption coefficient; $B_\nu(T_e)$ the Planck function; and $h\nu$ the photon energy in units of keV. The ratio of the x ray to neutron yield is then independent of the hot spot density, volume, and burn width, and scales only with temperature, shell attenuation, and mix fraction:

$$\frac{X_\nu}{Y_{\mathrm{DT}}} \simeq \frac{4\pi}{f_D f_T A_v^2 \langle \sigma_{\mathrm{DT}} v(T_i) \rangle} \frac{e^{-h\nu/kT_e}}{(h\nu)^{0.33}} \left(1 + \sum x_i Z_i\right) \\ \times \left(1 + \sum x_i \frac{j_i}{j_{\mathrm{DT}}}\right) e^{-\tau_\nu^{\mathrm{shell}}} (\mathrm{erg/Hz}). \quad (4)$$

The neutron yield and ion temperature are measured by a suite of neutron time-of-flight detectors [27], neutron activation diagnostics [28], and the magnetic recoil spectrometer [29]. Hot spot volume is determined from gated

2D x-ray imagers measuring the spatial emission profiles along two orthogonal lines of sight, and the burn duration is measured by the same gated detectors as well as a streaked x-ray camera [30,31]. The x-ray emission from the hot spot is measured by two diagnostics: the Ross Pair Imager and South Pole Bang Time (SPBT). The Ross Pair diagnostic [32,33] employs differential filtering [34] to provide time-integrated, x-ray self-emission images of the imploded core in five energy channels starting at 6 keV and above. As these five filters span the low energy region of the spectrum sensitive to ablator attenuation, up to the higher energies which suffer little attenuation, a simultaneous fit to the signal levels measured through each filter provides a measurement of both shell attenuation and x-ray emission enhancement.

The simplifying assumptions underlying Eq. (4) are that the nuclear and x-ray emission volumes and burn durations are the same, and $T_e = T_i$. Then, using the measured values of Y_{DT} and T_i, we use Eq. (4) to calculate the unattenuated x-ray emission spectrum from a no mix, "clean" pure DT hot spot. This spectrum is convolved with the filter transmission of each Ross channel and the image plate detector response. The best fit values for the shell optical depth, $\tau_\nu^{\mathrm{shell}}$, and the $(1 + \sum x_i Z_i)$ $[1 + \sum x_i (j_i/j_{\mathrm{DT}})]$ enhancement factor are then found by the reduced χ^2 minimization method. In the case of CH mix, $Z_C = 6$, $Z_H = 1$, and we obtain $x \equiv x_C = x_H$. The CH mix mass is then given by

$$\mathrm{mass_{CH}} = \frac{x(A_C + A_H)}{A_{\mathrm{DT}}} \mathrm{mass_{DT}} = x \frac{13}{2.5} \mathrm{mass_{DT}}, \quad (5)$$

using the DT hot spot mass calculated from Eq. (1). Typical calculated hot spot masses for the set of DT implosions were 3.8 ± 1.5 μg. The impact of the approximations of the model, and of systematic uncertainties in the fusion reaction rates, x-ray opacities, and absolute detector responses, are ameliorated by normalizing relative to the cleanest shot and setting it to have a nominal mix mass of 30 ng. This value represents the expected contribution to mix from the capsule fuel fill tube, as estimated by simulations [35]. Changing this value up or down would result in a relative scaling of the mix mass inferred for the other shots. The main uncertainty in the calculated enhancement ratio and mix fraction then arises from the uncertainty in the shell attenuation. We estimate this error as $2 \times \min(\chi^2)$. This is propagated to calculate the reported error in the mix mass in nanograms. While this method has a large uncertainty for low mix shots (mix mass $\lesssim 150$ ng), the uncertainty decreases with increasing mix.

The SPBT diagnostic records the temporally resolved x-ray emission in a narrow band at 10.85 ± 0.3 keV [36,37]. When corrected for shell attenuation (by using the optical depth derived from the Ross Pairs), the SPBT signal gives an additional measurement of the x-ray to neutron yield ratio and, hence, using the same method as before, the CH mix mass.

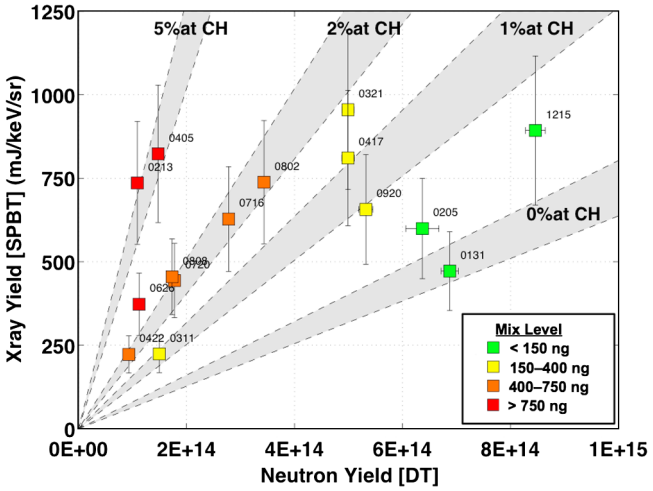

FIG. 2 (color online). X-ray yield (as measured by SPBT) versus neutron yield for the layered NIF implosions. Gray bands show percentages of atomic CH mix into the clean DT over the range of ion temperatures of 1.7–3.9 keV represented by this set of shots.

Figure 2 plots the measured 10.85 keV hot spot x-ray yield from the SPBT diagnostic, corrected for shell attenuation, versus the measured DT neutron yield for the layered implosions performed on the NIF. The gray bands are the theoretical x-ray to neutron yield ratios from Eq. (4) for a clean hot spot and mix ratios of $x = 1\%$, 2%, and 5% atomic mix from the ablator into the hot spot. The width of each band represents the ion temperature range $1.7 < T_i < 3.9$ keV, and indicates the relatively weak dependence of the ratio on temperature.

Figure 3 shows the observed DT neutron yield versus the inferred mix mass for the database of cryogenic DT

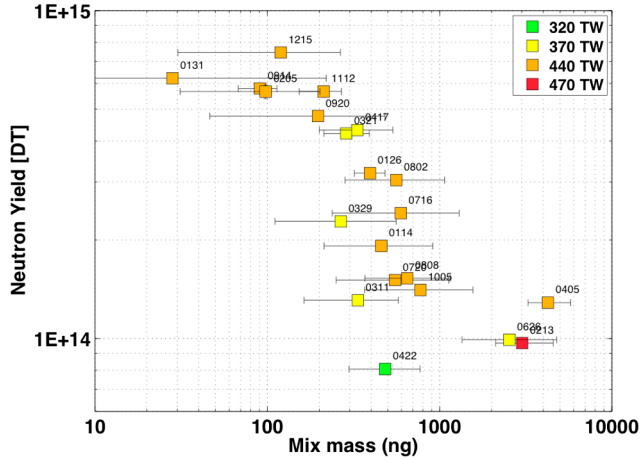

FIG. 3 (color online). DT neutron yield versus inferred mix mass for the layered implosions. Points are color coded by peak laser power. The 25 TW increase in effective peak power when DU hohlraums are used [43] is accounted for here.

implosions completed on the NIF. We observe the highest Y_n for shots with mix masses of below 200 ng, and yield performance dropping steeply just beyond that. Details of each shot, such as differences in peak laser power, fourth pulse slope and duration, hohlraum materials, capsule dopant concentrations, and capsule surface defects, influence the actual measured level of mix and account for the scatter in the data set. As shown, the bulk of our shots have employed peak powers of 370–440 TW, over which we observe large variability in the amount of measured mix. We also did a low power shot of 320 TW and a high power shot of 470 TW (pulse shapes shown in Fig. 1). Both implosions showed substantial mix. It is possible that the decreased classical growth due to lower acceleration with the lower power shot was not enough to overcome the decreased ablative stabilization. In the case of the high peak power shot, likely the increased x-ray drive resulted in a thinner ablator during the acceleration phase, increasing susceptibility to instability feedthrough. Simulations of these shots are exploring the plausibility of these hypotheses. We have also examined the yield versus mix mass relation across a large number of other shot attributes and in most cases find only weak trends. One persistent trend is that only shots with a truncated fourth pulse lie in the low mix region. These pulses reduce the late time acceleration of the shell and allow it to decompress, reducing ablation front growth rates and the level of instability feedthrough.

Figure 4 plots the experimentally measured DT neutron yield against T_i for the ensemble of layered shots. It shows that the reduction in T_i as the yield decreases is more gradual than predicted by the $Y_{\mathrm{DT}} \sim T_i^{4.7}$ theoretical scaling for the 1D neutron yield in the absence of alpha deposition [38]. Simulations that are perfectly spherical

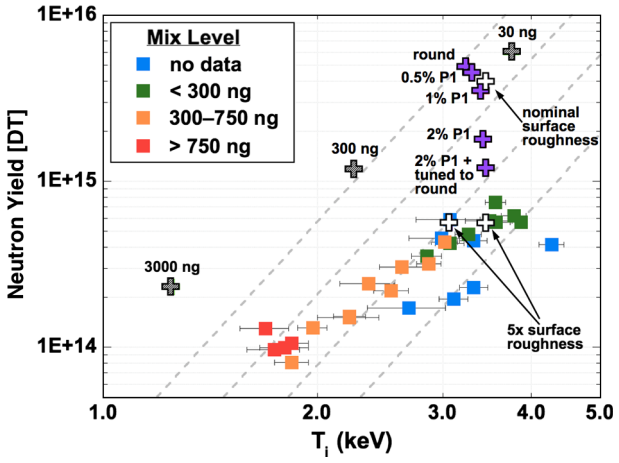

FIG. 4 (color online). Experimental DT neutron yield versus T_i (solid squares) distinguished by level of mix. Dashed lines represent the expected $Y_{\mathrm{DT}} \sim T_i^{4.7}$ power scaling [38] for constant hot spot densities. Open crosses are 2D HYDRA simulations for a 370 TW drive with surface roughness increased to match yield and T_i; filled (purple) crosses vary the P1 asymmetry; hatched (gray) crosses include artificially enhanced mix.

and have no mix dramatically over-estimate the yield, while giving an ion temperature comparable to the upper limit of what is experimentally observed. Postshot 2D radiation-hydrodynamic HYDRA [39] simulations, using our current knowledge of drive asymmetries, capsule and ice surface roughness, and approximations for the effect of the fill tube and capsule support tent, typically predict DT neutron yields that are higher than experimentally observed by factors of 5–10 [40]. However, the data trend is reproduced when artificially enhanced mix is included in simulations, as is seen by the gray hatched crosses that represent 30, 300, and 3000 ng of CH preloaded into the DT gas. While the simulations still overpredict the yield as compared to the data, we can recover the correct slope, demonstrating that radiative cooling through mix plays a significant role in explaining the performance.

To account for uncertainties in simulations of the RT instability, we have performed calculations with the initial surface perturbations arbitrarily increased until the yield is similar to observed. These simulations show reasonable agreement with the observed low-mix yield and ion temperature. The two indicated simulations with 5× surface roughness (open crosses in Fig. 4) differ in assumed detailed shape of the initial roughness. These simulations also agree with the observed areal density, and with the sizes of the x-ray and neutron images.

Further, modeling in which low mode perturbations are applied (solid purple crosses in Fig. 4) also tend to bring the simulations closer to the experimental data [41]. These simulations impose a radiation drive with a P_1 Legendre mode asymmetry of 0.5%, 1%, and 2%, which progressively decrease the yield, while incrementally increasing the T_i. These drive asymmetries result in a heavily disturbed cold fuel, with the hot spot displaced, reducing the central pressure. As P_1 is difficult to diagnose experimentally (requiring absolute knowledge of hot spot location relative to hohlraum or radiation drive), a P_1 asymmetry may appear as a P_2 or P_3 in images of the neutrons or x-ray self-emission (which originate from the low pressure region). Attempting to correct for P_2 and P_3 in the hot spot could further reduce yield by 2 ×.

Imaging of the hot spot emission shows that these 3D low-mode asymmetries can be significant (see Fig. 1), and recent backlit radiography of the in-flight shell shows even more pronounced shape and ρR asymmetries [42].

A number of mix mitigation techniques are presently being pursued, including reducing the seeds for RT growth by fabricating smoother capsules, and modifying the capsule design, possibly with thicker ice and thicker ablators. In addition, laser pulse shape tuning to increase the strength of the initial shock is expected to provide increased RT ablative stabilization. This, however, comes with a tradeoff of raising the adiabat of the target due to the increased shock heating and lowers the final fuel pressure. Effects of the intrinsic perturbation introduced by the

capsule support tent and other large scale nonuniformities are also being investigated.

It should be noted that the degree of uniformity of mix in the hot spot is not well known at this time. There are several mechanisms for bringing ablator material into the hotspot, ranging from mid-to-high mode hydrodynamic instabilities at the ablation front or fuel-ablator interface to jets from capsule surface defects or the fill tube [35]. In our method, we assume the mix is uniformly distributed to calculate the average atomic mix fraction of CH to DT; however, the calculation is valid to a good degree even if the CH is strongly localized, provided that the isobaric pressure and temperature equilibrium conditions are maintained in the hot spot volume. Further, our measurements showing the onset of the mix cliff at several hundred nanograms of mix agrees with the estimates in our point design [8].

In summary, we have developed a model that uses the ratio of the experimentally measured level of elevated x-ray emission to neutron yield to quantify the impurity mix of the shell ablator into the hot spot. Applying this model to the full ensemble of indirect-drive NIF cryogenically layered DT implosions to date has defined strong performance degradation at levels of several hundred nanograms of mix mass, consistent with expected sensitivity to the mix. The high velocity, high convergence conditions demonstrated have resulted in an increased hydrodynamic mix of the ablator into the hot spot. Simulations with increased surface roughness or imposed low mode asymmetries can bring the predicted yields and ion temperatures close to agreement with experimental observations, and ongoing experiments are focused on reducing these perturbations to improve the implosion performance.

We wish to thank the NIF operations team. This work was performed under the auspices of the U.S. Department of Energy by Lawrence Livermore National Laboratory under Contract No. DE-AC52-07NA27344.

[1] S. H. Glenzer *et al.*, Phys. Plasmas **19**, 056318 (2012).
[2] M. J. Edwards *et al.*, Phys. Plasmas **18**, 051003 (2011).
[3] G. H. Miller, E. I. Moses, and C. R. Wuest, Nucl. Fusion **44**, S228 (2004).
[4] J. Nuckolls, L. Wood, A. Thiessen, and G. B. Zimmerman, Nature (London) **239**, 139 (1972).
[5] S. Atzeni and J. Meyer-Ter-Vehn, *The Physics of Inertial Fusion* (Oxford Science, New York, 2004).
[6] B. K. Spears *et al.*, Phys. Plasmas **19**, 6316 (2012).
[7] O. L. Landen *et al.*, Phys. Plasmas **18**, 051002 (2011).
[8] S. W. Haan *et al.*, Phys. Plasmas **18**, 051001 (2011).
[9] H. F. Robey *et al.*, Phys. Rev. Lett. **108**, 215004 (2012).
[10] H. F. Robey *et al.*, Phys. Plasmas **19**, 042706 (2012).
[11] L. Rayleigh, *Scientific Papers II* (Cambridge University Press, Cambridge, England, 1900), p. 200.
[12] G. Taylor, Proc. R. Soc. London **201**, 192 (1950).
[13] R. D. Richtmyer, Commun. Pure Appl. Math. **13**, 297 (1960).
[14] E. E. Meshkov, Soviet Fluid Dyn. **4**, 101 (1969).
[15] L. Kelvin, Philos. Mag. **4**, 362 (1871).
[16] H. von Helmholtz, Monthly Reports of the Royal Prussian Academy of Philosophy in Berlin **23**, 215 (1868).
[17] J. D. Lindl, P. Amendt, R. L. Berger, and S. G. Glendinning, S. H. Glenzer, S. W. Haan, R. L. Kauffman, O. L. Landen, and L. J. Suter, Phys. Plasmas **11**, 339 (2004).
[18] N. M. Hoffman, *Proceedings of the 45th Scottish Universities Summer School in Physics, St Andrews, August 1994, Laser Plasma Interactions 5: Inertial Confinement Fusion*, edited by M. B. Hooper (Institute of Physics Publishing, New York, 1995), p. 105.
[19] T. Boehly, J. Delettrez, J. Knauer, D. Meyerhofer, B. Yaakobi, R. Town, and D. Hoarty, Phys. Rev. Lett. **87**, 145003 (2001).
[20] J. D. Kilkenny, S. G. Glendinning, S. W. Haan, B. A. Hammel, J. D. Lindl, D. Munro, B. A. Remington, S. V. Weber, J. P. Knauer, and C. P. Verdon, Phys. Plasmas **1**, 1379 (1994).
[21] S. V. Weber, B. A. Remington, S. W. Haan, B. G. Wilson, and J. K. Nash, Phys. Plasmas **1**, 3652 (1994).
[22] B. A. Remington, S. V. Weber, M. M. Marinak, S. W. Haan, J. D. Kilkenny, R. J. Wallace, and G. Dimonte, Phys. Plasmas **2**, 241 (1995).
[23] S. P. Regan *et al.*, Phys. Plasmas **19**, 056307 (2012).
[24] M. H. Key and R. J. Hutcheon, Adv. At. Mol. Phys. **16**, 201 (1980).
[25] F. J. Rogers, F. J. Swenson, and C. A. Iglesias, Astrophys. J. **456**, 902 (1996).
[26] H. A. Scott and S. B. Hansen, High Energy Density Phys. **6**, 39 (2010).
[27] V. Y. Glebov *et al.*, Rev. Sci. Instrum. **81**, 10D325 (2010).
[28] D. L. Bleuel *et al.*, Rev. Sci. Instrum. **83**, 10D313 (2012).
[29] D. T. Casey *et al.*, Rev. Sci. Instrum. **83**, 10D912 (2012).
[30] S. Glenn *et al.*, Rev. Sci. Instrum. **81**, 10E539 (2010).
[31] S. F. Khan *et al.*, in *SPIE Optical Engineering + Applications*, edited by P. Bell and G. P. Grim (SPIE, Bellingham, WA, 2012), p. 850505.
[32] T. Ma *et al.*, Rev. Sci. Instrum. **83**, 10E115 (2012).
[33] N. Izumi *et al.*, Rev. Sci. Instrum. **83**, 10E121 (2012).
[34] P. Ross, J. Opt. Soc. Am. **16**, 433 (1928).
[35] B. A. Hammel *et al.*, Phys. Plasmas **18**, 056310 (2011).
[36] A. G. MacPhee *et al.*, JINST **6**, P02009 (2011).
[37] D. H. Edgell *et al.*, Rev. Sci. Instrum. **83**, 10E119 (2012).
[38] R. Betti, P. Y. Chang, B. K. Spears, K. S. Anderson, J. Edwards, M. Fatenejad, J. D. Lindl, R. L. Mccrory, R. Nora, and D. Shvarts, Phys. Plasmas **17**, 058102 (2010).
[39] M. M. Marinak, G. D. Kerbel, N. A. Gentile, O. Jones, D. Munro, S. Pollaine, T. R. Dittrich, and S. W. Haan, Phys. Plasmas **8**, 2275 (2001).
[40] D. S. Clark *et al.*, Phys. Plasmas **20**, 056318 (2013).
[41] B. K. Spears, D. S. Clark, M. J. Edwards, S. W. Haan, J. D. Lindl, D. H. Munro, L. J. Suter, and C. A. Thomas, Bull. Am. Phys. Soc. **57**, 112 (2012).
[42] R. Rygg, Phys. Plasmas (to be published).
[43] D. A. Callahan *et al.*, Phys. Plasmas **19**, 6305 (2012).